



# Surface structure and topology in surface stabilized Co-nanoparticles with a thin Al<sub>2</sub>O<sub>3</sub> amorphous layer

S. Rana<sup>a</sup>, S. Ram<sup>a,\*</sup>, S. Seal<sup>b</sup>, S.K. Roy<sup>c</sup>

<sup>a</sup>Materials Science Centre, Indian Institute of Technology, Kharagpur-721302, India

<sup>b</sup>AMPAC and MMAE, University of Central Florida, Orlando, FL 32816-2455, USA

<sup>c</sup>Department of Metallurgical and Materials Engineering, Indian Institute of Technology, Kharagpur-721302, India

Received 19 September 2003; received in revised form 14 April 2004; accepted 14 April 2004

Available online 10 June 2004

## Abstract

Heating an amorphous Co<sup>2+</sup>:AlO(OH)· $\alpha$ H<sub>2</sub>O gel under a reducing atmosphere of pure H<sub>2</sub> gas at 700–850 °C temperature results in surface stabilized Co-metal nanoparticles with a thin Al<sub>2</sub>O<sub>3</sub> ceramic surface layer. At early temperatures during heating, the gel decomposes and disperses in a refined structure in divided Co<sup>2+</sup> groups through a matrix of Al<sub>2</sub>O<sub>3</sub> (amorphous). A reconstructive Co<sup>2+</sup> + H<sub>2</sub> → Co + 2H<sup>+</sup> reaction operates in the divided groups to result in isolated Co-particles. Formation and existence of Al<sub>2</sub>O<sub>3</sub> layer (in a limited thickness  $t \leq R_0$ , with  $R_0 \sim 4.28$  nm the critical Al<sub>2</sub>O<sub>3</sub> dimension to grow as a stable crystallite) over growing Co-particles control the process in a high-energy metastable fcc or bcc Co allotrope structure. Average crystallite size thus hardly grows to be as big as 41 nm. A large value of surface energy  $\sigma = 0.790$  J/m<sup>2</sup> in Al<sub>2</sub>O<sub>3</sub>, in comparison to 0.234 J/m<sup>2</sup> in fcc or 0.279 J/m<sup>2</sup> in hcp Co, inhibits a moderate diffusion of surface atoms and in turn controls the nucleation and growth in small Co-particles. Otherwise, a particle of pure Co metal grows rapidly in the hcp bulk structure. The results of the Al<sub>2</sub>O<sub>3</sub> surface modified fcc and bcc Co are analyzed with X-ray photoelectron spectroscopy in correlation of X-ray diffraction and microstructure.

© 2004 Published by Elsevier B.V.

**Keywords:** Surface topology; Phase transformation; Surface modified Co-nanoparticles; Nanocermet; XPS analysis; Microstructure; X-ray diffraction

## 1. Introduction

Surface modification and encapsulation of size selected metal particles are a subject of immense interest due to their unique structural, magnetic and other physical properties, which make them very

appealing both from theoretical and technological points of view [1–7]. Pure Co metal in bulk form has an hcp crystal structure with a martensitic transformation to an fcc structure at  $\sim 427$  °C temperature [1,3]. The fcc Co also exists at ambient temperature if the size is reduced to few nanometers [2,5]. Prinz synthesized Co granules in a bcc allotrope by epitaxial growth in thin films over GaAs [8]. Ram reported this phase to exist in small crystallites of  $D = 2–5$  nm diameter [5]. Such small particles have rapid surface

\* Corresponding author. Tel.: +91-322-228-3980;

fax: +91-322-225-5303.

E-mail address: [sram@matsec.iitkgp.ernet.in](mailto:sram@matsec.iitkgp.ernet.in) (S. Ram).

oxidation due to the large surface area. This can be controlled by a thin surface coating of  $\text{Al}_2\text{O}_3$  or other inert ceramics [5,9–11].

Several methods have been developed to synthesize nanoparticles and clusters of Co, Ni, or Fe metal [12–14]. Clusters of 40–500 atoms obtained by laser vaporization are usually “naked”, with no surface layer of other species. They have an enhanced magnetization, usually 5–30%, in comparison to the bulk value [13,14]. Chemical methods, including the Rieke method [15], the inverse micelle technique [2,16], or the sonochemical method [17], provide alternative ways for synthesizing separated metal particles. Particles prepared with a chemical route often have a thin surface layer of other species, leaving scope for prevention of surface oxidation in air. Moreover, the physical and chemical properties are substantially modified in coated particles [16,17]. Co-nanoparticles so produced have the fcc structure [17–19]. A few groups have succeeded in encapsulating small metal particles in carbon nanotubes [7,20–22].

Undesirably, carbon reacts with the metal particles to form carbides [20–22], which, being to be non-magnetic or weakly magnetic, hamper the prospects of the encapsulation. Surface stabilized metal particles in elemental state with a ceramic surface layer offer several advantages for applications in magnetic energy storage, magnetic recording, magnetic resonance imaging and ferrofluids [16–22]. A thin  $\text{Al}_2\text{O}_3$  surface layer, 2–4 nm in thickness ( $t$ ), over a Co-nanoparticle effectively insulates it by forming an insulator surface barrier. It establishes a magnetic tunnel junction (MTJ) between two Co-particles separated by the barrier layer, exhibiting tunneling magnetoresistance (TMR). A 6–30% value of TMR lies at room temperature [9,10], with promising applications in magnetic random access memories, read heads, and sensors.

This article reports the structure and topology in surface stabilized Co-nanoparticles with a thin  $\text{Al}_2\text{O}_3$  surface layer. The  $\text{Al}_2\text{O}_3$  layer supports a metastable fcc or bcc Co structure. The Co: $\text{Al}_2\text{O}_3$  samples are synthesized by thermal decomposition and reconstructive co-reduction reaction under different conditions from a  $\text{Co}^{2+}:\text{AlO}(\text{OH})\cdot\alpha\text{H}_2\text{O}$  gel. The results are analyzed with the microstructure, X-ray diffraction, and X-ray photoelectron spectroscopy (XPS).

## 2. Experimental details

The encapsulated Co-nanoparticles in amorphous  $\text{Al}_2\text{O}_3$  thin films,  $t \leq 4$  nm, were synthesized from an amorphous  $\text{Co}^{2+}:\text{AlO}(\text{OH})\cdot\alpha\text{H}_2\text{O}$  gel. On heating under  $\text{H}_2$  gas, the gel decomposes into a refined precursor of dispersed  $\text{Co}^{2+}$  cations in the matrix of an amorphous  $\text{Al}_2\text{O}_3$  (porous) over 150–350 °C temperature. A co-reduction reaction,  $\text{Co}^{2+} + \text{H}_2 \rightarrow \text{Co} + 2\text{H}^+$ , follows at higher temperatures, resulting in surface stabilized Co-nanoparticles with a thin  $\text{Al}_2\text{O}_3$  surface layer at 700–850 °C. A schematic diagram illustrating the whole procedure of the synthesis is given in Fig. 1. The samples were obtained of different  $D$  values by heating the precursor at different temperatures. A freshly prepared precursor gel has been used in this experiment. As described earlier [5,16], it was synthesized by hydrolysis of an aqueous  $\text{CoCl}_2\cdot 6\text{H}_2\text{O}$  solution in reaction with an Al-metal at room temperature.

X-ray diffraction of Co: $\text{Al}_2\text{O}_3$  was studied with P.W. 1710 X-ray diffractometer using Co  $K\alpha$  radiation of wavelength  $\lambda = 0.17902$  nm. Surface structure of

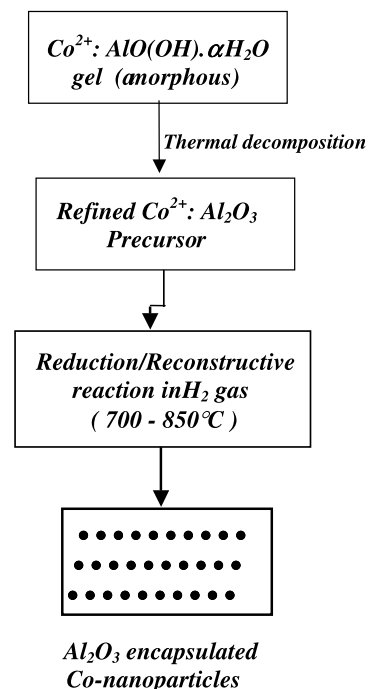


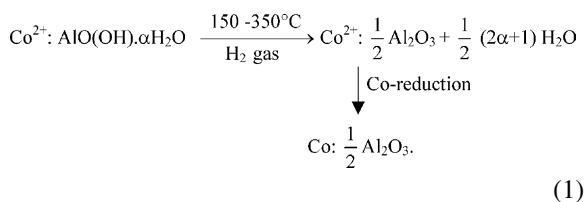
Fig. 1. A schematic diagram in the processing of surface modified Co-nanoparticles with a thin  $\text{Al}_2\text{O}_3$  ceramic surface layer.

Co-nanoparticles coated with thin Al<sub>2</sub>O<sub>3</sub> film was analyzed through XPS studies. The microstructure was studied with a scanning electron microscope (SEM) of JEOL model JSM-5800 and a transmission electron microscope (TEM) of model-JEM 2000 CX. Compositional analysis, carried out with an energy dispersive X-ray (EDX) analyzer (in conjunction with SEM) shows no significant impurity except a small trace of ~1 at.% even smaller due to carbon. The sample in TEM analysis was prepared by dispersing powder in alcohol over an ultrasonic bath. A drop of suspension was placed with a syringe on a carbon coated copper grid, which was ultimately loaded with sample in the microscope for the analysis. Average *D* value has been calculated from widths  $\Delta 2\theta_{1/2}$  in X-ray diffraction peaks with the Debye Scherrer relation [23].

### 3. Results and discussion

#### 3.1. X-ray diffraction in allotropes in Co-nanoparticles

As described in Fig. 1, on heating in H<sub>2</sub> gas, the Co<sup>2+</sup>:AlO(OH)·H<sub>2</sub>O gel decomposes at temperatures as early as 150–350 °C, resulting in a dispersed structure of Co<sup>2+</sup> cations in the matrix of Al<sub>2</sub>O<sub>3</sub> (amorphous). It reflects in an endothermic signal with absorption of as large heat as ~925 J/g, in DSC thermal analysis [5]. The decomposition profile, as studied with thermal analysis, varies as a function of composition and content of chemisorbed water ( $\alpha$ ) in the sample. A value of  $\alpha = 3.0$  is estimated by thermogravimetric analysis for the sample of ~50 wt.% Co as per the final Co:Al<sub>2</sub>O<sub>3</sub> composition. An efficient co-reduction reaction,  $\text{Co}^{2+} + \text{H}_2 \rightarrow \text{Co} + 2\text{H}^+$ , occurs of dispersed Co<sup>2+</sup> in small groups in Al<sub>2</sub>O<sub>3</sub> at 700–850 °C temperature as follows:



Reaction (1) occurs in a controlled fashion in divided reaction centers in Al<sub>2</sub>O<sub>3</sub> matrix at expense of the excess volume  $\Delta V$  (or Gibbs free energy  $\Delta G$ ) over the

equilibrium value. In this process, the Al<sub>2</sub>O<sub>3</sub> reacts with nascent surfaces in the resulting Co-particles and thus encapsulates the Co-particles in thin Al<sub>2</sub>O<sub>3</sub> layer(s). The number of Al<sub>2</sub>O<sub>3</sub> layers in the coating over a Co-particle thus depends on the Co–Al<sub>2</sub>O<sub>3</sub> surface reaction, which, in turn, is determined by the total surface energy and thickness in the interface in the Co:Al<sub>2</sub>O<sub>3</sub> particle. As a result, the *t* value is self-controlled within a few Al<sub>2</sub>O<sub>3</sub> molecular layers. It governs a controlled growth of coated Co-particles by improving the effective surface energy  $\sigma$ , which governs diffusion of the reaction species through the interface. A modified Co surface with an improved  $\sigma$  value (in comparison to 0.234 J/m<sup>2</sup> in fcc Co [24] or 0.279 J/m<sup>2</sup> in hcp Co [24], with  $\sigma = 0.790$  J/m<sup>2</sup> in  $\gamma$ -Al<sub>2</sub>O<sub>3</sub> [25]) in this example renders a self-controlled diffusion of surface atoms during an early growth stage of Co:Al<sub>2</sub>O<sub>3</sub> particles. As a matter of fact, a high-energy metastable fcc or bcc Co results in support of the modified surface as discussed below in terms of the X-ray diffraction.

X-ray diffractograms (Fig. 2) in Co:Al<sub>2</sub>O<sub>3</sub> samples (50 mass% Co) co-reduced from a Co<sup>2+</sup>:AlO(OH)· $\alpha$ H<sub>2</sub>O gel after heating at (a) 700 °C for 30 min, (b) 700 °C for 30 min and then 30 min at 850 °C, and (c) 850 °C for 30 min have a total of six peaks, in the 45–105° range of  $2\theta$ , due to fcc and bcc Co. These peaks are as sharp as of  $\Delta 2\theta_{1/2} \leq 0.36^\circ$ . Variation in their relative intensities demonstrates a variation in  $f_{\text{fcc}}$  and  $f_{\text{bcc}}$  volume fractions in the two phases in three samples. The temperature and the time period used in the heating are selected by optimizing a monolithic Co phase. According to the peak intensities (integrated), the fcc phase is the prominent phase, with  $f_{\text{fcc}} \sim 65, 56, \text{ or } 85\%$  in the respective samples (Table 1).

There are significant variations also in the peak positions (interplanar spacings  $d_{hkl} = \lambda/2 \sin \theta$ ) and  $\Delta 2\theta_{1/2}$  values in the three samples. The  $d_{hkl}$  and  $\Delta 2\theta_{1/2}$  values are used to estimate lattice parameters *a* and average *D* values in the two fcc and bcc Co phases (Tables 1 and 2). The lattice volume  $V = a^3$  and the lattice surface energy  $\Omega = A\sigma$ , with  $A = 6a^2$  the lattice surface area, are included in Table 2. A value of  $a = 0.3547, 0.3548, \text{ or } 0.3550$  nm (in comparison to the 0.3547 nm bulk value<sup>1</sup>) is found in  $D = 41, 36, \text{ or}$

<sup>1</sup> X-ray powder JCPDS diffraction files (a) 5.0727, hcp Co, (b) 15.806, fcc Co, and (c) 29.63,  $\gamma$ -Al<sub>2</sub>O<sub>3</sub>.

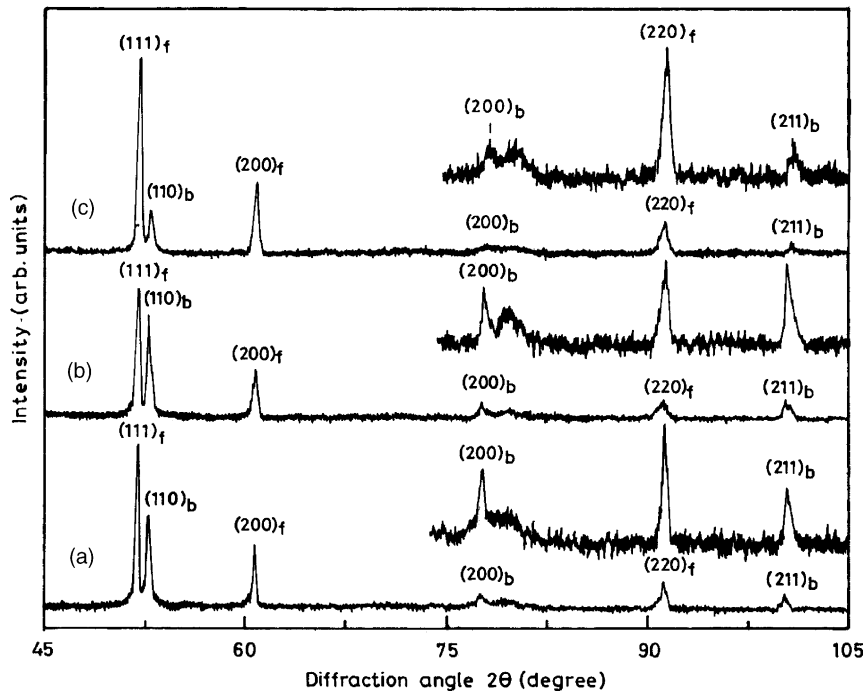


Fig. 2. X-ray diffractograms in  $\text{Al}_2\text{O}_3$  surface modified Co-nanoparticles deduced by heating the gel at (a)  $700^\circ\text{C}$ , (b)  $700^\circ\text{C}$  followed by  $850^\circ\text{C}$ , and (c)  $850^\circ\text{C}$  in  $\text{H}_2$  gas for 30 min at each of the final temperatures. Parts of diffractograms reproduced at a magnified intensity scale clarify the weak bands. The fcc and bcc Co peaks are marked by letters of f and b along with  $(hkl)$  values.

34 nm particles in the fcc Co in three samples, respectively. In bcc Co,  $a = 0.2855$ ,  $0.2859$ , or  $0.2849$  nm, with  $D = 48$ ,  $42$ , or  $36$  nm, respectively. Earlier, a further smaller value of  $a = 0.2840$  nm has been reported in as big as  $D = 80$  nm bcc Co crystallites embedded in a similar amorphous  $\text{Al}_2\text{O}_3$  matrix [5].

The bcc Co obtained in this example is not so stable allotrope of cobalt as the fcc one. It forms at effectively low temperatures as  $700^\circ\text{C}$  in support of the

$\text{Al}_2\text{O}_3$  coating in divided particles. This confirms involvement of a smaller value of effective  $\sigma$  (eases diffusion of the reaction species) in formation of it than in the fcc or hcp Co allotrope (Table 2). At a given processing temperature, a maximum  $D$  value (Table 1) thus lies in this specific allotrope. Forming a stable  $\text{Al}_2\text{O}_3$  coating over growing Co particles, during the heating in  $\text{H}_2$  gas, controls the final size and morphology in the bcc or fcc Co allotrope, which involves an

Table 1

Volume fractions and average crystallite sizes in Co-nanoparticles in fcc and bcc allotropes with a thin  $\text{Al}_2\text{O}_3$  surface layer prepared by co-reducing a  $\text{Co}^{2+}:\text{AlO}(\text{OH})\cdot x\text{H}_2\text{O}$  gel in  $\text{H}_2$  gas under different conditions

Sample	Volume fraction (%)		Crystallite size (nm)	
	fcc	bcc	fcc	bcc
1. Co-reduced at $700^\circ\text{C}$ (30 min)	65	35	41	48
2. Sample (1) heated 30 min at $850^\circ\text{C}$	56	44	36	42
3. Co-reduced at $850^\circ\text{C}$ (30 min)	85	15	34	36

The samples have 50 mass% Co. The volume fractions in the two phases are determined from intensities in the X-ray diffraction peaks while the crystallite size is estimated from the peak-widths. The reported values of volume fraction or the crystallite size are accurate within  $\pm 2\%$  error of the measurements.

Table 2

Lattice parameter  $a$  or  $c$ , lattice surface area  $A$ , lattice volume  $V$ , and lattice surface energy  $\Omega$  in Co-nanoparticles in fcc and bcc allotropes with a thin  $\text{Al}_2\text{O}_3$  surface layer

Sample	Lattice parameter <sup>a</sup> , $a$ (nm)	$A$ ( $\times 10^{-2}$ nm <sup>2</sup> )	$V$ ( $\times 10^{-3}$ nm <sup>3</sup> )	$\Omega$ ( $\times 10^{-20}$ J) <sup>b</sup>
1. Co-reduced at 700 °C (30 min)				
fcc structure	0.3547	75.49	44.63	17.66
bcc structure	0.2855	48.91	23.27	9.98
2. Sample (1) heated at 850 °C (30 min)				
fcc structure	0.3548	75.53	44.66	17.67
bcc structure	0.2859	49.04	23.37	10.00
3. Co-reduced at 850 °C (30 min)				
fcc structure	0.3550	75.62	44.74	17.70
bcc structure	0.2849	48.70	23.12	9.93
4. Bulk cobalt metal				
fcc structure	$a = 0.3547^c$	75.49	44.63	17.66
hcp structure	$a = 0.2507, c = 0.4070^c$	93.90	66.50	26.20

<sup>a</sup> The reported  $a$  or  $c$  values have  $\pm 0.0005$  nm error of the measurements.

<sup>b</sup> The value of  $\Omega = A\sigma$  is calculated with  $\sigma = 0.234$  J/m<sup>2</sup> for fcc Co and 0.279 J/m<sup>2</sup> for hcp Co in Ref. [24]. In the absence of a reported  $\sigma$  value for bcc Co, it is assumed to be the same as 0.204 J/m<sup>2</sup> for the bcc Fe in Ref. [24].

<sup>c</sup> The lattice parameters for bulk Co are reported from footnote 1.

adequately moderate value of  $\Omega$  energy of  $10.0 \times 10^{-20}$  or  $17.7 \times 10^{-20}$  J, depending on the final temperature and other experimental conditions. Otherwise, at such high temperatures, a pure Co sample readily grows in the hcp structure [5], with a much larger value of  $\Omega = 26.2 \times 10^{-20}$  J (Table 2). The coated bcc Co in  $\text{Al}_2\text{O}_3$  in separate particles converts to the fcc Co in 30 min of heating at as high temperatures as 900 °C in  $\text{H}_2$  gas.

In general, small fcc or bcc Co crystallites have a correlation between  $a$  and  $D$  such that a manifested  $a$  value lies at  $D \leq D_c$ , with  $D_c$  the critical  $D$  value at which the surface atoms become effective in determining the final distribution of the atoms in the sample. As proposed by Gleiter [26], this correlation supports the fact that the surface atoms in such small crystallites suffer from a reduced value of (i) atomic density (or an enhanced interatomic distance), (ii) coordination number, or (iii) symmetry than those in the core. Thus, Co crystallites of a confined size,  $D \leq D_c$ , have a reasonably manifested  $V$  value over the bulk value. This would be feasible as long as the surface atoms (impart a relatively high structural energy) do not undergo a redistribution by optimizing the total energy. This occurs at  $D$  below  $D_c^*$ , where  $D_c^*$  refers to the critical value at which the surface atoms become

compatible to the core atoms and dominate the activity of the sample as quantum dot.

A Co-nanoparticle,  $D_c^* < D \leq D_c$ , thus can be regarded of consisting of two structural parts: a crystalline component (CC) of core atoms and an inter-crystalline component (IC) of surface atoms. The IC region is extended in the sample with a thin  $\text{Al}_2\text{O}_3$  surface layer(s). It includes the Co– $\text{Al}_2\text{O}_3$  surface interface layer. A difference in interatomic distances, if any, in the two regions could appear in a splitting in the X-ray diffraction peaks. It is seen indeed in a high-resolution diffractogram in (1 1 1) and (1 1 0) reflections in Figs. 3 and 4 in the fcc and bcc Co samples, respectively. As marked by the letters of I and II, the two distinct overlapping components are split up in either example. As expected, relative intensities vary in two components depending on the lattice reflection, the lattice structure, and the crystallite size. A deconvolution of the observed peak profile reproduces the two components of near Gaussian shapes (the dashed curves). Computed value of integrated intensity in the two peaks (with the fit parameters given in Tables 3 and 4) reproduces the observed value within a maximum  $\pm 5\%$  deviation.

The kind of the splitting observed in X-ray diffraction peaks in this example should not be confused with

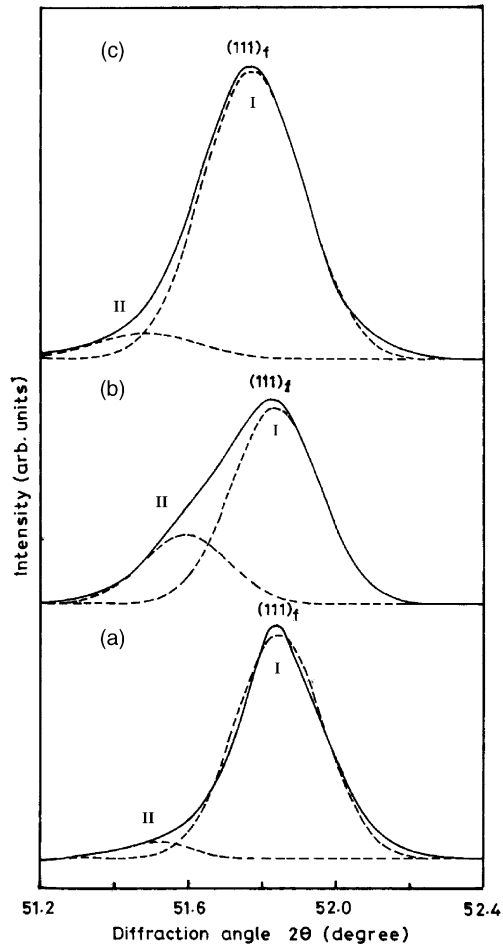


Fig. 3. A high-resolution X-ray diffractogram with its deconvolution in two peaks in (1 1 1) reflection in fcc Co-nanoparticles in the three samples in Fig. 2.

a possible splitting due to the difference in wavelengths in the X-ray source of  $\text{Co K}\alpha_1$  and  $\text{Co K}\alpha_2$  radiations used to measure the diffractogram. The difference in these two wavelengths,  $\Delta\lambda = 0.0003885 \text{ nm}$  [27], is too small to reflect in a splitting in broadened peaks in small crystallites as in this example. In order to confirm it further, we studied high-resolution X-ray diffractograms in selected  $(hkl)$  peaks for pure  $\alpha\text{-Al}_2\text{O}_3$  of similar 30–50 nm  $D$  values, with no such distinct splitting [28]. Using a smaller  $\lambda = 0.15405 \text{ nm}$  value of  $\text{Cu K}\alpha_1$  (with a similar  $\Delta\lambda = 0.0003828 \text{ nm}$  difference from the  $\text{Cu K}\alpha_2$  value [27]), does show some asymmetry in peaks at high  $2\theta$  values of  $70^\circ$  or still larger. In this case, the

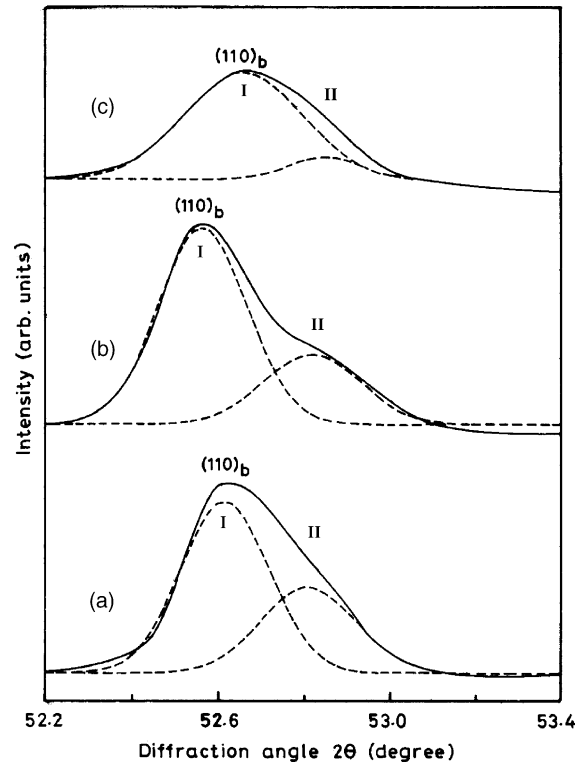


Fig. 4. A high-resolution X-ray diffractogram with its deconvolution in two peaks in (1 1 0) reflection in bcc Co-nanoparticles in the three samples in Fig. 2.

Table 3

Initial peak-width  $\Delta 2\theta_{1/2}$ , effective  $D$  and deconvolution parameters in (1 1 1) X-ray diffraction peak in fcc Co-nanoparticles with a thin  $\text{Al}_2\text{O}_3$  surface layer

Sample	$\Delta 2\theta_{1/2}$ ( $^\circ$ )	Peak	Peak position ( $^\circ$ )	Peak-width ( $^\circ$ )	Effective $D$ (nm)
Sample 10.235		I	51.85	0.237	43
		II	51.52	0.176	
Sample 20.350		I	51.84	0.238	42
		II	51.59	0.230	
Sample 30.285		I	51.78	0.271	37
		II	51.49	0.273	

The samples 1–3 are the same as in Table 1 or Table 2. The effective  $D$  value is calculated from  $\Delta 2\theta_{1/2}$  in the prominent peak I in the CC component. The error of the measurement is  $\pm 2\%$  in  $\Delta 2\theta_{1/2}$  or the derived parameters.

Table 4

Initial peak-width  $\Delta 2\theta_{1/2}$ , effective  $D$  and deconvolution parameters in (1 1 0) X-ray diffraction peak in bcc Co-nanoparticles with a thin  $\text{Al}_2\text{O}_3$  surface layer

Sample	$\Delta 2\theta_{1/2}$ ( $^\circ$ )	Peak	Peak position ( $^\circ$ )	Peak-width ( $^\circ$ )	Effective $D$ (nm)
Sample 1	0.350	I	52.62	0.211	48
		II	52.82	0.228	
Sample 2	0.335	I	52.56	0.244	42
		II	52.84	0.275	
Sample 3	0.340	I	52.66	0.281	36
		II	52.84	0.176	

The samples 1–3 are the same as in Table 1. The effective  $D$  value is calculated from  $\Delta 2\theta_{1/2}$  in the prominent peak I in the CC component. The error of the measurement is  $\pm 2\%$  in  $\Delta 2\theta_{1/2}$  or the derived parameters.

component of the higher  $2\theta$  value lies as a satellite peak according to the  $\text{Cu K}\alpha_2$  intensity, which is very weak as compared to the  $\text{Cu K}\alpha_1$  value (smaller  $\lambda$ -component). The ratio in intensities in the two peaks does not vary much from sample to sample with a function of  $D$  value as analyzed in  $\text{Co:Al}_2\text{O}_3$  cermets as follows.

In Fig. 3, peak I, which is prominent in intensity in (1 1 1) reflection, refers to the CC region while peak II refers to the IC region. Peak II lies (as a satellite peak) in improved  $d_{hkl}$  of 0.2060, 0.2057, or 0.2061 nm relative to average position in the primary peak I of 0.2047, 0.2048, or 0.2050 nm in three fcc Co samples, respectively. In the bcc Co samples, in Fig. 4, the (1 1 0) reflection presents an opposite trend in displacing of average position of peak II relative to the position in the primary peak I. Thus, peak II lies at smaller  $d_{hkl}$  as 0.2013, 0.2012, or 0.2011 nm respect to 0.2019, 0.2021, or 0.2018 nm in peak I.

Relative intensity (integrated) in peak II varies as a function of fractional volume  $f_{ic}$  of IC region. A maximum  $f_{ic}$  value is found to be 34% in bcc Co in sample (a) in Fig. 4. A value of  $f_{ic} = 29\%$  lies in sample (b) while that of 10% in sample (c). In general, a relatively smaller  $f_{ic}$  value, i.e. 5, 25, or 8% lies in the three samples of fcc Co, respectively (Fig. 3). The results imply that the  $f_{ic}$  value is a complicated function of (i) the specific surface area, (ii) the  $\sigma$  value, (iii) the atomic packing factor  $\Phi$ , and (iv) the chemistry of the sample. It can be argued that a smaller value of  $\Phi = 0.68$ , or  $\sigma = 0.204 \text{ J/m}^2$ , in the bcc Co in com-

parison to  $\Phi = 0.74$ , or  $\sigma = 0.234 \text{ J/m}^2$ , in the fcc Co favors a more closely packed IC redistribution over the CC region by retaining on average the bcc structure. This occurs by minimizing the total energy of the  $\text{Co:Al}_2\text{O}_3$  particle in a metastable thermodynamic state. This is the reason that the  $d_{hkl}$  in IC region has improved value (with a smaller  $\Phi$  than in the CC region) in the fcc Co while an adversely diminished value (with a larger  $\Phi$  than in the CC region) in the bcc Co relative to that in the CC regions.

In order to examine whether the IC influences the final particle structure in an isotropic manner (i.e., improves its crystal symmetry [5,26]), another example of X-ray diffractogram is studied of (2 0 0) reflection of fcc Co-nanoparticles. This particular reflection (Fig. 5), which involves {2 0 0} planes perpendicular to the  $a$ -axis [1 0 0], does not show a distinct splitting in two components. Moreover, the signature of a

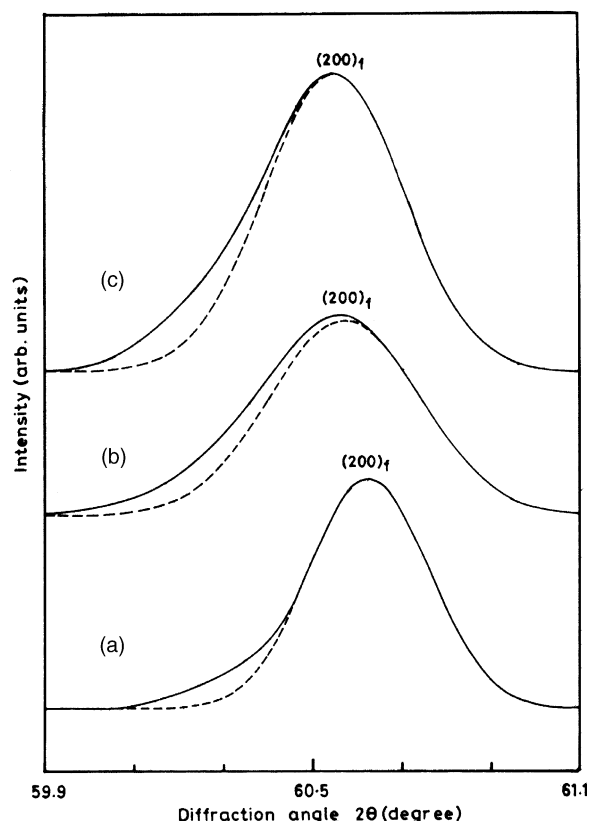


Fig. 5. A high-resolution X-ray diffractogram and its deconvolution with a Gaussian shape in (2 0 0) reflection in fcc Co-nanoparticles in the three samples in Fig. 2.

Table 5  
Deconvolution parameters in (2 0 0) X-ray diffraction peak in fcc Co-nanoparticles with a thin Al<sub>2</sub>O<sub>3</sub> surface layer

Sample	Peak position (°)	Peak-width (°)	Effective <i>D</i> (nm)
Sample 1	60.62	0.275	38
Sample 2	60.56	0.364	29
Sample 3	60.54	0.343	31

The samples 1–3 are the same as in Table 1. The error of the measurement is  $\pm 2\%$  in  $\Delta 2\theta_{1/2}$  or the derived parameters.

deviation of atomic distribution from that in the CC region is very much reflected in asymmetric shape of the peak, with the value of  $\Delta 2\theta$  of (a) 0.275°, (b) 0.364°, and (c) 0.343° in the three samples (Table 5). Average  $d_{hkl}$  in this peak varies very little as 0.17736, 0.17752, or 0.17757 nm in these samples, respectively. The core dominates an anisotropic growth of Co-nanoparticles. A change in anisotropy of the surface energy in clean metal crystals on adsorption of foreign atoms is well known [18]. It stabilizes one or more of the crystal planes with a strong faceting. For example, Pt particles develop sharply faceted shapes with large (1 1 1), (1 0 0) and (1 1 0) faces if covered with carbon [18].

The results infer further that the degree of IC atomic redistribution over the CC region depends on the morphology of growth in the Co-crystallites. According to the intensity distribution in X-ray diffractograms in Fig. 2, the most preferred direction of growth is [1 1 1] in the fcc Co while [1 1 0] in the bcc Co. As a result, a maximum density of number of planes lies in (1 1 1) planes in the fcc Co samples whereas in the (1 1 0) planes in the bcc Co samples. Obviously, this is the reason that these two specific reflections appear with a maximum change in IC atomic redistribution in the diffractograms in Figs. 2–4.

### 3.2. Structure in thin Al<sub>2</sub>O<sub>3</sub> surface layer

The Al<sub>2</sub>O<sub>3</sub> in these Co:Al<sub>2</sub>O<sub>3</sub> powders has an amorphous structure. It adds no distinct peak(s) in the X-ray diffractogram in Fig. 2. In general, Al<sub>2</sub>O<sub>3</sub> has several polymorphs, which are easily identified with their characteristic X-ray diffractograms. In heating an Al<sub>2</sub>O<sub>3</sub> precursor such as AlO(OH)· $\alpha$ H<sub>2</sub>O [29],

the polymorph  $\gamma$ -Al<sub>2</sub>O<sub>3</sub> derives at as early temperatures as 400–800 °C in air. It has a total of seven X-ray diffraction peaks at 0.4530 (1 1 1), 0.2800 (2 2 0), 0.2390 (3 1 1), 0.2280 (2 2 2), 0.1980 (4 0 0), 0.1530 (5 1 1) and 0.1400 nm (4 4;0), with  $a = 0.7924$  nm in an O<sub>H</sub><sup>7</sup>-F<sub>D3M</sub> cubic crystal structure (see footnote 1). The (4 4 0) reflection lies in the most intense peak of the diffractogram. These peaks are not present here in the Co:Al<sub>2</sub>O<sub>3</sub> X-ray diffractograms.

Amorphous Al<sub>2</sub>O<sub>3</sub>, which coats Co-nanoparticles, is highly stable and does not recrystallize under these conditions. Thermodynamically, on heating over such high temperatures (700–850 °C), such high-energy structure is possible to retain as such if and only if Al<sub>2</sub>O<sub>3</sub> is extremely thin ( $t < 2r_c$ ) in supported strain layers with high-energy Co-surfaces in small Co:Al<sub>2</sub>O<sub>3</sub> particles. The strain energy in thin Al<sub>2</sub>O<sub>3</sub> layers supports high-energy amorphous state of Al<sub>2</sub>O<sub>3</sub>. In principle, a solid nucleates and grows in a specific crystal structure if and only if it succeeds to attain a critical dimension  $2r_c$  ( $r_c = 2\sigma/\Delta G_v$  radius in a spherical shape) [30]. A value of  $r_c = 2.14$  nm is calculated using  $\sigma = 0.790$  J/m<sup>2</sup>, with  $\Delta G_v = 0.74 \times 10^9$  J/m<sup>3</sup> the Gibbs free-energy of  $\gamma$ -Al<sub>2</sub>O<sub>3</sub> formation from an amorphous state [30]. So, the Al<sub>2</sub>O<sub>3</sub> film would retain an amorphous structure as long as it is supported with the Co-surface and does not grow above the critical  $t_c = 2r_c \cong 4.28$  nm value. An interconnected network structure forms of Al<sub>2</sub>O<sub>3</sub> and intimately adheres to the metal surface with strong Co–Al<sub>2</sub>O<sub>3</sub> chemical bonding through O<sup>2-</sup> ions.

It is quite possible that a thin Al<sub>2</sub>O<sub>3</sub> surface layer in Co:Al<sub>2</sub>O<sub>3</sub> nanocermetts also adds a significant counter-part strain in the lattice in part of the specimen of encapsulated Co-metal particles. Two types of strains are possible in this case. One is the macrostrain due to which the characteristic X-ray diffraction peaks get shifted towards higher  $d_{hkl}$  values and the other is the microstrain, which induces peak broadening [31]. Their effects become increasingly important in decreasing *D* to a few nanometers [32]. An analysis of them is an independent exercise and it will be reported separately. In Fig. 6, a plot of  $\beta \cos \theta/\lambda$  versus  $\sin \theta/\lambda$ , in the relation [33]:

$$\frac{\beta \cos \theta}{\lambda} = \frac{1}{D} + \frac{\eta \sin \theta}{\lambda} \quad (2)$$

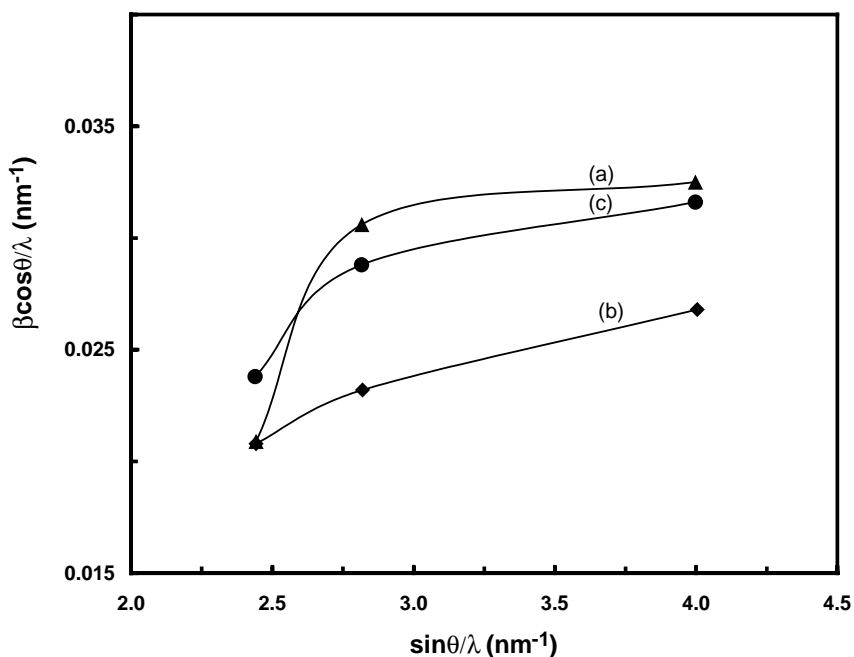


Fig. 6.  $\beta \cos \theta/\lambda$  vs.  $\sin \theta/\lambda$  plots, with average  $\eta$  value of (a) 0.0034, (b) 0.0045 and (c) 0.0037, in the three samples in Fig. 2.

gives a very small value of effective strain  $\eta$  of 0.0034–0.0045 (with  $\pm 0.0002$  the error bar) in the linear part over  $\sin \theta/\lambda$  above 2.8 in the three Co:Al<sub>2</sub>O<sub>3</sub> samples. The  $\beta = \Delta 2\theta_{1/2}$ ,  $\cos \theta$  and  $\sin \theta$  values are taken for the (1 1 1), (2 0 0) and (2 2 0) X-ray diffraction peaks of fcc Co. A nonlinear deviation of the data points (especially in the (1 1 1) peak of small  $\sin \theta/\lambda$  value) from an ideal straight-line plot in this equation demonstrates that there is nonuniform strain along the different crystallographic orientations. This lies in departure from uniform particle shape and in turn in the departure from uniform IC and CC distributions along the different crystallographic orientations. The [1 1 1] orientation thus faces a maximum strain in these three orientations.

Obviously, the contribution of  $\eta$  in the total  $\Delta 2\theta_{1/2}$  is not much in comparison to the direct effect of size  $D$  in the individual Co particles. For all other practical purposes, it can be ignored here in the cases of effectively large Co particles of  $D \geq 34$  nm. This simplifies the parameters in computing average  $D$  value by the measured  $\Delta 2\theta_{1/2}$  in primary X-ray diffraction peaks in the CC component in Al<sub>2</sub>O<sub>3</sub> coated Co particles as given in Tables 3–5.

### 3.3. Microstructure in Al<sub>2</sub>O<sub>3</sub> surface stabilized Co-nanoparticles

SEM micrographs in Fig. 7a and b have near spherical shapes of Al<sub>2</sub>O<sub>3</sub> surface stabilized Co particles of average  $d \sim 300$  nm diameter. Both of them are taken from the same sample (heated at 700 °C for 30 min from the gel) at two magnifications to present the topology of smooth surfaces. In Fig. 7c, a modified morphology of ellipsoidal particles lies, with a smaller value of  $d \sim 150$  nm, in another sample processed at higher temperature 850 °C. A thermally activated reaction occurs in refined precursor species by driving the process with a rather fast growth of Al<sub>2</sub>O<sub>3</sub> surface layer to an effective  $t$  value so that it controls the final growth to be more effectively in encapsulated Co-particles. The present value of  $d$  is roughly as larger as 5–8 times the  $D$  value determined from the  $\Delta 2\theta_{1/2}$  values. The difference in the two values envisages that Al<sub>2</sub>O<sub>3</sub> encapsulated Co crystallites are grown in form of the clusters.

It can be argued that a spherical or a modified ellipsoidal shape in a cluster particle results from originally spherical shape of basic structural compo-

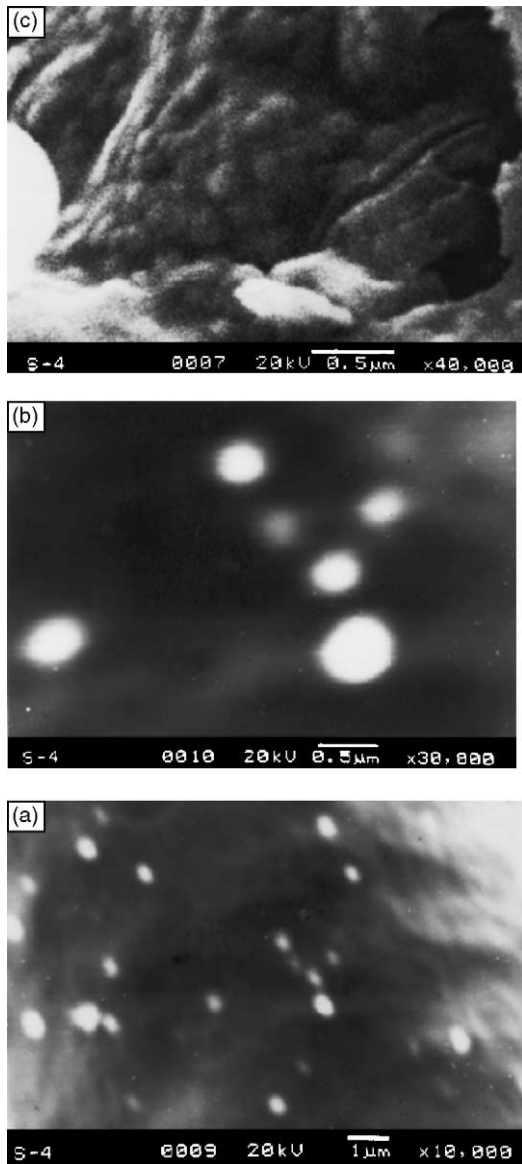


Fig. 7. SEM micrographs in  $\text{Al}_2\text{O}_3$  surface modified Co-nanoparticles processed by heating the gel at (a) or (b) 700, and (c) 850 °C in  $\text{H}_2$  gas.

nents BSCs ( $\text{Al}_2\text{O}_3$  surface modified Co-crystallites) in preponderance of the  $\Omega$  energy. A controlled growth by migration of the Co reaction species through the surface in a growing Co particle renders it to be in spherical shape as it involves a minimum  $\Omega$  value. Under the constraints of the  $\text{Al}_2\text{O}_3$  surface barrier, the BSCs prefer to recombine in clusters in order to

optimizing the average  $\Omega$  value. A spherical crystallite of radius  $1/2D$  involves  $\Omega_g = 4\pi(1/2D)^2\sigma \div 4/3\pi(1/2D)^3\rho \equiv 6\sigma(D\rho)^{-1}$ , i.e.,  $\Omega_g = 4.698 \text{ J/g}$  at  $D = 34 \text{ nm}$  in the fcc Co, with  $\sigma = 0.234 \text{ J/m}^2$  and density  $\rho = 8.79 \text{ g/cm}^3$ . Here,  $\Omega_g$  refers to  $\Omega$  for grains. This is larger in magnitude than the change in the enthalpy  $\Delta H = 4.24 \text{ J/g}$  in the hcp  $\rightarrow$  fcc transformation in bulk Co [19]. Thus, it is not feasible for Co to exist in the fcc structure at so large  $\Omega_g$  value unless it is stabilized by a high  $\sigma$ -valued surface layer. A further reduced  $\Omega_c = 1.065 \text{ J/g}$  value, i.e. as much as by a factor of 5, of crystallites lies in cluster in as small  $d$  as 150 nm. It has as many crystallites as 86 of  $D = 34 \text{ nm}$ .

According to the microstructure (Fig. 7), an effectively improved  $\Omega_g$  value in modified Co metal surface with  $\text{Al}_2\text{O}_3$  surface barrier layer ( $\sigma \sim 0.790 \text{ J/m}^2$ ) promotes high-energy BSCs to arrange in a close packed structure in clusters. The  $\text{Al}_2\text{O}_3$  renders the interbridging by chemical bonding via  $\text{O}^{2-}$  in common interfaces in the BSCs. A small  $\sigma$  increase, that is to the value of hcp Co of  $\sigma = 0.279 \text{ J/m}^2$ , thus may lead the initial fcc structure to exist irrespective to dimension in encapsulated Co particles. The results not only demonstrate that the Co-nanoparticles are encapsulated in thin  $\text{Al}_2\text{O}_3$  layers but also suggest that the metallic surface supports a high-energy amorphous  $\text{Al}_2\text{O}_3$  structure in thin layers,  $t < t_c$ , otherwise it gets recrystallized during heating at so high temperatures. There is report that encapsulating Co or other metal nanoparticles in carbon promotes graphitization of the carbon-coating in thin layers [21].

TEM images in a typical Co: $\text{Al}_2\text{O}_3$  sample (heated 30 min at 700 °C followed by 30 min at 850 °C in  $\text{H}_2$  gas from gel) have near cubical or rectangular shapes of particles of 30–40 nm diameter (Fig. 8a). These small particles represent the BSCs (crystallites) which somehow did not grow as clusters. We analyzed TEM images from different regions of this sample, with the result of a fairly sharp size distribution of crystallites. About 90% crystallites lie in the 30–40 nm range of size. The kind of the cubical shape observed here in Co crystallites is not common. It might be the result of controlled growth in fcc or bcc Co structures in small crystallites under the influence of a strained Co– $\text{Al}_2\text{O}_3$  surface layer with an effectively large  $\Omega$  value. Cubic shape of particles has been reported in fine ceramics such as monodispersed  $\text{ZrO}_2$  [34,35]. In the corre-

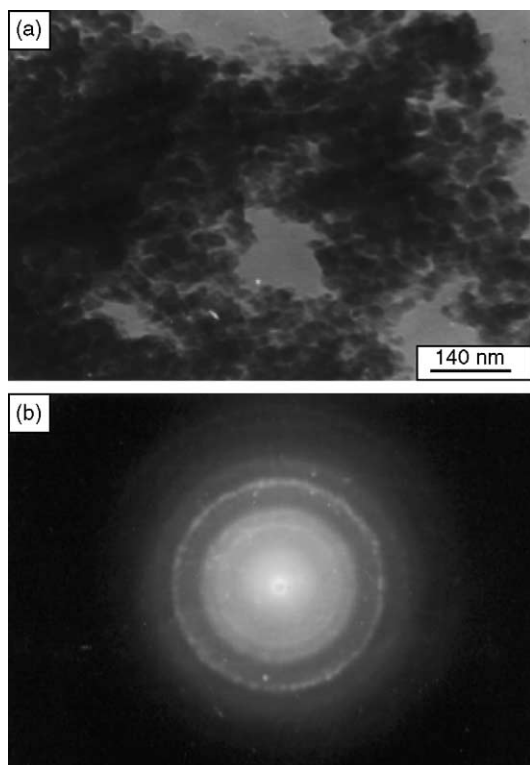


Fig. 8. (a) TEM micrograph and (b) the corresponding electron diffractogram in Co:Al<sub>2</sub>O<sub>3</sub> sample deduced in 30 min of heating at 700 °C and then 30 min at 850 °C from gel in H<sub>2</sub> gas.

sponding electron diffractogram of the Co:Al<sub>2</sub>O<sub>3</sub> sample in Fig. 8b, four distinct rings lie in 0.2060, 0.2025, 0.1780 and 0.1245 nm of  $d_{hkl}$  in favorable values in the X-ray diffractogram (Fig. 2b) in (1 1 1), (2 0 0) and (2 2 0) reflections at 0.2048, 0.1775 and 0.1253 nm in the fcc Co and in (1 1 0) reflection at 0.2021 nm in the bcc Co.

A sequence of layers of coating of carbon on a metal-particle had been seen in high-resolution electron micrograph (HREM) images [20]. They contain many crystalline defects [20]. A similar structure of distorted grain boundaries lies in HREM in Co-nanoparticles,  $D = 13\text{--}15$  nm, produced by mechanical attrition [19]. A distorted grain boundary is seldom found in coarse grains. It is intrinsic of small particles with high-energy surface defects. In Co:Al<sub>2</sub>O<sub>3</sub> nanocermet, this has been cured by surface reaction with Al<sub>2</sub>O<sub>3</sub>. A thin Co–Al<sub>2</sub>O<sub>3</sub> surface interface thus forms at expense of the excess energy in integral part of Co-

particle in a specific structure, resulting in a uniform contrast throughout the particle with a smoothed surface topology (Fig. 7b).

It is clear that effective  $D$  and  $\Omega$  values determine stability of Co-particles in a specific allotrope. Sato et al. [2] studied fcc  $\rightarrow$  hcp transformation in pure fcc Co prepared by sputtering method. The transformation is found to be suppressed in  $D = 10$  nm particles. On milling, in an inert gas atmosphere, a bulk Co powder follows a sequence of hcp + fcc  $\rightarrow$  hcp, hcp + fcc  $\rightarrow$  hcp  $\rightarrow$  fcc + hcp, and hcp + fcc  $\rightarrow$  hcp  $\rightarrow$  fcc + hcp  $\rightarrow$  fcc transformations. These are induced basically by a refinement of microstructure with addition of a large amount of structural energy in defects, imperfections and high angle grain boundaries during the milling process [19]. A self-reorganization of structure follows with creation of new surfaces in a way that it encounters a minimal change of the free energy. In this process, the fcc Co, which involves a reduced  $V$  of hcp Co by 33 % (Table 2), thus forms first in a metastable structure at limited  $D \leq 22$  nm [19].

The surface stabilized Co-nanoparticles with a thin Al<sub>2</sub>O<sub>3</sub> surface layer in this example are peculiarly substantially stable in the fcc or bcc structure to a rather large  $D = 50\text{--}100$  nm value. Obviously, (i) their modified surfaces with an improved  $\sigma$  and (ii) the Co–Al<sub>2</sub>O<sub>3</sub> surface interface or barrier layer are the two key factors, which extend and lend support for their improved thermodynamic stability in such large dimensions. Otherwise, they convert to the hcp structure at much lower  $D \leq 22$  nm [19]. The results are useful in stabilizing and designing of novel supported metal nanoparticles, cermet, or metal reinforced nanoceramic composites.

#### 3.4. XPS in Al<sub>2</sub>O<sub>3</sub> surface stabilized Co-nanoparticles

XPS is applied in order to confirm surface structure of Co-nanoparticles, which are encapsulated in thin Al<sub>2</sub>O<sub>3</sub> layers. It is a very sensitive analytical technique to study the surfaces of materials down to a few atomic layers from the surface [36]. Fig. 9 shows the XPS spectrum (a) for sample 3 (heated 30 min at 850 °C), which has a maximum of 85% fcc Co in a phase mixture with 15% bcc Co. A spectrum (b) in sample 2 (heated 30 min at 850 °C after 30 min at 700 °C), of a bit smaller fcc Co content of 66%, is given in the inset

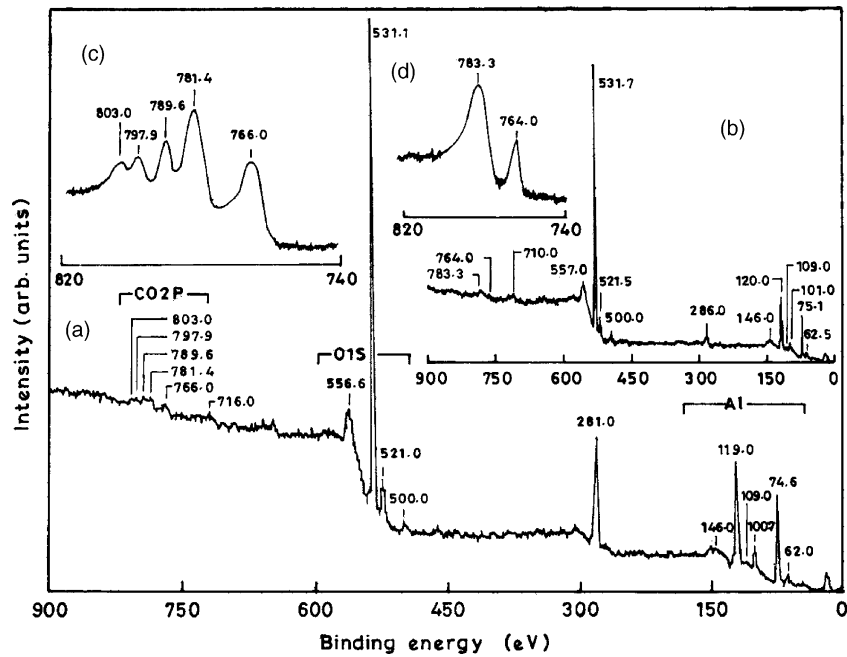


Fig. 9. XPS spectra in  $\text{Al}_2\text{O}_3$  surface modified Co-nanoparticles processed by heating from gel at (a) 850 and (b) 700 °C followed by 850 °C in  $\text{H}_2$  gas. A close-up of parts of spectra in (a) and (b) is given in (c) and (d), respectively. Weak Co bands in the two regions are resolved after smoothing the data and subtracting the background.

Table 6

XPS bands in fcc Co rich samples of Co-nanoparticles with a thin  $\text{Al}_2\text{O}_3$  surface layer

Sample 2		Sample 3		Assignments
Peak position (eV)	Intensity	Peak position (eV)	Intensity	
62.5	2	62.0	2	$\text{Al}2\text{p}_{3/2}$ ( $\text{Al}_{\text{III}}\text{-O}$ )
75.1	16	74.6	17	$\text{Al}2\text{p}_{3/2}$ ( $\text{Al}_{\text{I}}\text{-O}$ )
101.0	2	100.7	5	$\text{Al}2\text{p}_{3/2}$ ( $\text{Al}_{\text{I}}\text{-O-Co}$ )
109.0	2	109.0	1	$\text{Al}2\text{s}$ ( $\text{Al}_{\text{III}}\text{-O}$ )
120.0	20	119.0	20	$\text{Al}2\text{s}$ ( $\text{Al}_{\text{I}}\text{-O}$ )
146.0	2	146.0	3	$\text{Al}2\text{s}$ ( $\text{Al}_{\text{I}}\text{-O-Co}$ )
286.0	9	281.0	20	$\text{C}1\text{s}$ (impurity)
500.0	4	500.0	2	$\text{O}1\text{s}$ ( $\text{O}_{\text{IV}}$ in interface)
521.5	6	521.0	7	$\text{O}1\text{s}$ ( $\text{O}_{\text{III}}$ in interface)
531.7	100	531.1	100	$\text{O}1\text{s}$ ( $\text{O}_{\text{I}}$ in $\text{Al}_2\text{O}_3$ )
557.0	7	556.6	8	$\text{O}1\text{s}$ ( $\text{O}_{\text{II}}$ in interface)
710.0	~1	716.0	~1	$\text{Co}2\text{A}$ (Auger band)
764.0	~1	766.0	~1	$\text{Co}2\text{p}_{3/2}$ (bcc $\text{Co}_{\text{I}}$ )
783.3	~1	781.4	~1	$\text{Co}2\text{p}_{3/2}$ (fcc $\text{Co}_{\text{I}}$ )
		789.6	0.5	$\text{Co}2\text{p}_{3/2}$ (bcc-fcc $\text{Co}_{\text{II}}$ )
		797.9	0.3	$\text{Co}2\text{p}_{3/2}$ (bcc-fcc $\text{Co}_{\text{II}}$ )
		803.0	0.2	$\text{Co}2\text{p}_{3/2}$ (bcc-fcc $\text{Co}_{\text{II}}$ )

The samples 2 and 3 are the same as in Table 1.

in Fig. 9. Both the spectra are more or less the same with the most intense peak (peak intensity  $I_p = 100\%$ ) at 531.1 and 531.7 eV of binding energy  $E_b$ , respectively.  $I_p \leq 20\%$  in other peaks. All these peaks belong to  $O^{2-}$  and  $Al^{3+}$  of the Co:Al<sub>2</sub>O<sub>3</sub> sample. As the Al<sub>2</sub>O<sub>3</sub> layers cover the metal surface, no peak occurs from the Co metal surface, expected in the 760–815 eV range [36–39], in a significant  $I_p$  value.

A Co-nanoparticle with a Co–Al<sub>2</sub>O<sub>3</sub> surface interface has two types of Co atoms—one in the core and other in the interface. Pure Co metal has a characteristic 2p<sub>3/2</sub> band at 782.0 eV [36]. A close-up of spectrum (a) shows five bands in extremely small  $I_p \leq 1\%$  at 766.0, 781.4, 789.6, 797.9 and 803.0 eV as given in the inset (c) in Fig. 9. The first two bands are in 2p<sub>3/2</sub> excitation from the core Co<sub>I</sub> atoms in the bcc and fcc Co-nanoparticles, respectively. A small increase of 3.4% in average atomic volume (or decrease in the electron density) in the bcc Co lattice relative to the fcc Co one leads to shift the band at the lower  $E_b$  value. The other three Co band components, which lie at higher  $E_b$  values, possibly attribute to the Co<sub>II</sub> atoms in the Co–Al<sub>2</sub>O<sub>3</sub> interface. A more specific assignment of them is not feasible here in absence of the resolved features. An increased volume fraction of bcc Co phase of 44% in the other sample results in two distinct bands at 764.0 and 783.3 eV in spectrum (d) (in the inset in Fig. 9). Assignments of all the individual bands observed in the two samples are given in Table 6.

#### 4. Conclusions

A controlled co-reduction of dispersed Co<sup>2+</sup> cations by heating a Co<sup>2+</sup>:AlO(OH)· $\alpha$ H<sub>2</sub>O gel at 700–850 °C under H<sub>2</sub> gas results in Co-metal of small crystallites,  $D = 34$ – $41$  nm diameter, in fcc or bcc metastable crystal structure in support with a thin Co–Al<sub>2</sub>O<sub>3</sub> surface interface or Al<sub>2</sub>O<sub>3</sub> layer (amorphous) of thickness  $t$ . Clusters of Co-crystallites grow in near spherical or ellipsoidal shapes of diameter as large as 300 nm. The results are analyzed with microstructure, X-ray diffraction and XPS studies. The value of  $t$  is limited to the critical  $t_c = 2r_c$  value, with  $r_c$  the critical dimension in a stable Al<sub>2</sub>O<sub>3</sub> crystallite. A  $r_c = 2.14$  nm value is obtained, as per the  $r_c = 2\sigma/\Delta G_v$  relation, with  $\sigma = 0.790$  J/m<sup>2</sup> the surface energy and

$\Delta G_v = 0.74 \times 10^9$  J/m<sup>3</sup> the Gibbs free-energy of formation of  $\gamma$ -Al<sub>2</sub>O<sub>3</sub>.

A thin Al<sub>2</sub>O<sub>3</sub> surface layer over a growing Co-particle controls its growth in a high-energy metastable fcc or bcc phase in divided reaction centers. At early stage of the nucleation and growth, the nascent metal surface reacts with O atoms from Al<sub>2</sub>O<sub>3</sub> at the surface in a controlled way by forming a thin Co–Al<sub>2</sub>O<sub>3</sub> surface interface or barrier. An improved effective  $\sigma$  value over 0.234 J/m<sup>2</sup> in the fcc or 0.204 J/m<sup>2</sup> in the bcc Co, with  $\sigma = 0.790$  J/m<sup>2</sup> in Al<sub>2</sub>O<sub>3</sub>, inhibits a moderate surface diffusion of reaction species. Otherwise, the hcp bulk Co forms as the stable phase at an early  $D$  as 10–22 nm depending on the surface structure. Another advantage with the Co–Al<sub>2</sub>O<sub>3</sub> surface interface is that it insulates the Co-particle to form a surface tunneling barrier layer so that it offers the tunnel magnetoresistance [9,10].

As the Al<sub>2</sub>O<sub>3</sub> covers the metal surface, the XPS spectrum has extremely weak intensity,  $I_p \leq 1\%$ , in the Co bands with respect to  $I_p = 100\%$  in the most intense band at  $\sim 531$  eV in the 1s O<sup>2-</sup>. The results not only demonstrate that the Al<sub>2</sub>O<sub>3</sub> covers the metal surface in layers but also suggest that the metal surface supports the Al<sub>2</sub>O<sub>3</sub> in layers in a high-energy amorphous state. Thus, the Al<sub>2</sub>O<sub>3</sub> layer neither recrystallizes nor piles off the Co-metal surface till over as high temperatures as 850 °C in H<sub>2</sub> gas.

#### Acknowledgements

The authors gratefully acknowledge the financial support by a research grant from the DRDO (Defence Research and Development Organization) of Government of India.

#### References

- [1] J.P. Chen, C.M. Sorensen, K.J. Klabunde, G.C. Hadjipanayis, Phys. Rev. B 51 (1995) 11527.
- [2] H. Sato, O. Kitakami, T. Sakurai, Y. Shimada, Y. Otani, K. Fukamichi, J. Appl. Phys. 81 (1997) 1858.
- [3] M. Erbudak, E. Wetli, M. Hochstrasser, D. Pescia, D.D. Vvedensky, Phys. Rev. Lett. 79 (1997) 1893.
- [4] V. Russier, C. Petit, J. Legrand, M.P. Pileni, Phys. Rev. B 62 (2000) 3910.
- [5] S. Ram, Mater. Sci. Eng. A 304–306 (2001) 923.

- [6] X.L. Dong, C.J. Choi, B.K. Kim, *Scripta Mater.* 47 (2002) 857.
- [7] H. Bi, S. Li, X. Jiang, Y. Du, C. Yang, *Phys. Lett. A* 307 (2003) 69.
- [8] G.A. Prinz, *Phys. Rev. Lett.* 54 (1985) 1051.
- [9] J. Nassar, M. Hehn, A. Vaures, F. Petroff, A. Fert, *Appl. Phys. Lett.* 73 (1998) 698.
- [10] I.I. Oleinik, E.Y. Tsymbal, D.G. Pettifor, *Phys. Rev. B* 62 (2000) 3952.
- [11] J. Schmalhorst, H. Bruckl, M. Justus, A. Thomas, G. Reiss, M. Vieth, G. Gieres, J. Wecker, *J. Appl. Phys.* 89 (2001) 586.
- [12] M.L. Isabelle, J.A. Billas, J.A. Becker, A. Chatelain, W.A. Delteer, *Phys. Rev. Lett.* 71 (1993) 4067.
- [13] S.E. Apsel, J.W. Emmert, J. Deng, L.A. Bloomfield, *Phys. Rev. Lett.* 76 (1996) 1441.
- [14] S. Ram, H.J. Fecht, *Mater. Trans. JIM* 41 (2000) 754.
- [15] R.D. Rieke, *Crit. Rev. Surf. Chem.* 1 (1991) 131.
- [16] S. Ram, *J. Mater. Sci.* 35 (2000) 3561.
- [17] X.M. Lin, C.M. Sorensen, K.J. Klabunde, G.C. Hadjipanayis, *Langmuir* 14 (1998) 7140.
- [18] P.J.F. Harris, *Int. Mater. Rev.* 40 (1995) 97.
- [19] J.Y. Huang, Y.K. Wu, H.Q. Ye, *Acta Mater.* 44 (1996) 1201.
- [20] J.J. Host, M.H. Teng, B.R. Elliott, J.H. Hwang, T.O. Mason, D.L. Johnson, V.P. Dravid, *J. Mater. Res.* 12 (1997) 1268.
- [21] J. Jiao, S. Seraphin, *J. Appl. Phys.* 83 (1998) 2442.
- [22] E. Flahaut, F. Agnoli, J. Sloan, C. O'Connor, M.L.H. Green, *Chem. Mater.* 14 (2002) 2553.
- [23] L. Azaroff, *Elements of X-ray Crystallography*, McGraw-Hill, New York, 1968, p. 557.
- [24] D. Turnbull, *J. Appl. Phys.* 21 (1950) 1022.
- [25] J.M. Mchale, A. Auroux, A.J. Perrotta, A. Navrotsky, *Science* 277 (1997) 788.
- [26] H. Gleiter, *Acta Mater.* 48 (2000) 1.
- [27] B.D. Cullity, *Elements of X-ray Diffraction*, Addison-Wesley, London, 1978, p. 509.
- [28] S. Rana, S. Ram, *Phys. Stat. Sol. (a)* 201 (2004) 696.
- [29] S. Ram, S. Rana, *Mater. Sci. Eng. A* 304–306 (2001) 790.
- [30] A. Paul, *Chemistry of Glasses*, Chapman & Hall, London, 1990, pp. 326/367.
- [31] H.S. Nalwa, *Handbook of Nanostructured Materials and Nanotechnology*, vol. 2, Academic Press, 1994, p. 179.
- [32] K. Reimann, R. Wurschum, *J. Appl. Phys.* 81 (1997) 7186.
- [33] S.B. Qadri, E.P. Skelton, D. Hsu, A.D. Dinsmore, J. Yang, H.F. Gray, B.R. Ratna, *Phys. Rev. B* 60 (1999) 9191.
- [34] M.Z.C. Hu, R.D. Hunt, E.A. Payzant, C.R. Hubbard, *J. Am. Ceram. Soc.* 82 (1999) 2313.
- [35] A. Mondal, S. Ram, *J. Am. Ceram. Soc.*, in press.
- [36] G.E. Muilberg, *Handbook of X-ray Photoelectron Spectroscopy*, Perkin-Elmer, Eden Prairie, MN, 1979.
- [37] K.S. Kim, *Phys. Rev. B* 11 (1975) 2177.
- [38] S.S. Dhese, E. Dudzik, H.A. Durr, G.V. Laan, N.B. Brookes, *J. Appl. Phys.* 87 (2000) 5466.
- [39] M. Sato, S. Takada, S. Kohiki, T. Babasaki, H. Deguchi, M. Oku, M. Mitome, *Appl. Phys. Lett.* 77 (2000) 1194.